Supporting Information for

"Volcano-tectonic interactions at Sabancaya volcano, Peru: Eruptions, magmatic inflation, moderate earthquakes, and fault creep"

Patricia MacQueen[1], Francisco Delgado[1,2], Kevin Reath[1], Matthew E Pritchard[1], Marco Bagnardi[3*], Pietro Milillo[3], Paul Lundgren[3], Orlando Macedo[4], Victor Aguilar[4], Mayra Ortega[5], Rosa Anccasi[5], Ivonne Alejandra Lazarte Zerpa[5†], Rafael Miranda[5]

[1]Cornell University, Ithaca, New York, USA

[2]Equipe de Tectonique et Mécanique de la Lithosphère, Institut de Physique du Globe de Paris, Université de Paris

[3]Jet Propulsion Laboratory, California Institute of Technology, Pasadena, California, USA

[4]Universidad Nacional de San Agustín de Arequipa, Arequipa, Perú

[5]INGEMMET Volcano Observatory (OVI)

Contents

Introduction

This supplemental material provides additional information regarding the progression of eruptive activity at Sabancaya, InSAR modeling, additional interferograms, and seismicity in the central volcanic zone. We provide 10 figures and 2 tables.

*Now at: NASA Goddard Space Flight Center, Greenbelt, Maryland, USA

†Now at: Instituto Geofísico del Perú, Lima, Perú

Corresponding author: Patricia MacQueen, pgm65@cornell.edu

Figure S1

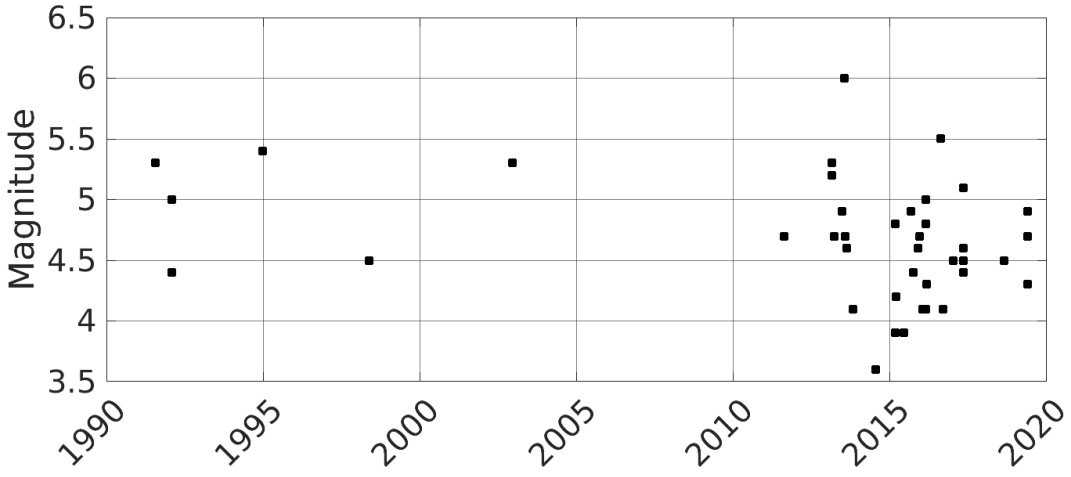

Figure S1. Earthquakes within 50 km of Sabancaya and less than 30 km depth from 1990 through 2019, from the NEIC Earthquake Database. Note that there are no earthquakes matching these constraints from 1950 to 1990 in the NEIC catalog. Magnitudes are a mix of types, all plotted together here for simplicity.

Figure S2

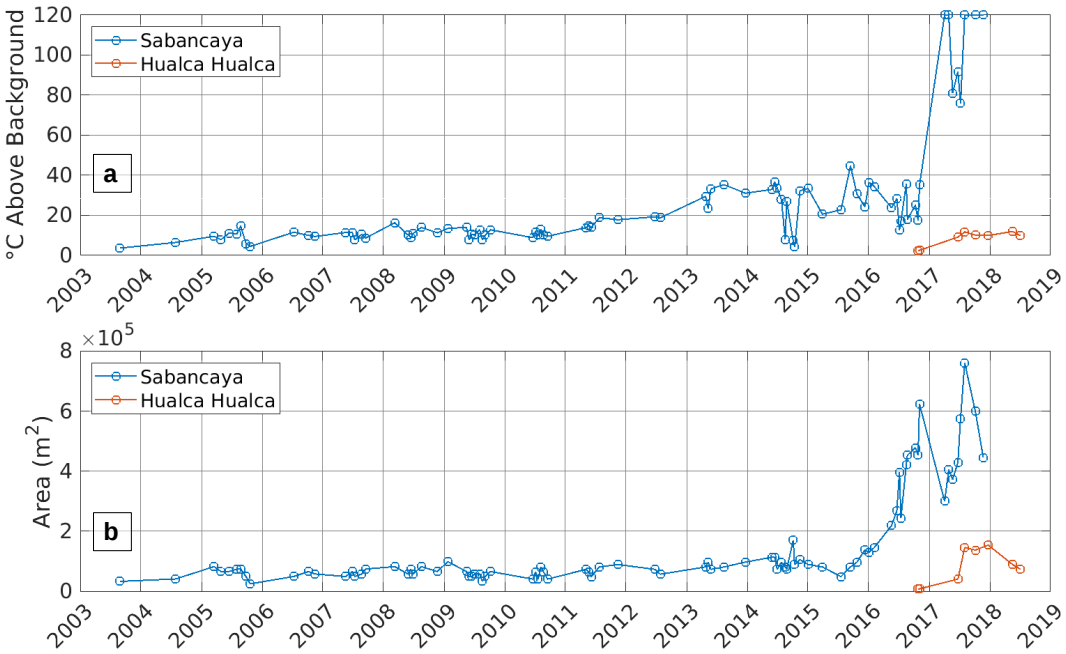

Figure S2. Temperature and area of ASTER thermal anomalies for Sabancaya and Hualca Hualca from 2003 to 2018. Temperature is the temperature above background of the hottest pixel, and area is the total sum of the anomalous pixel areas. The data for Sabancaya was previous published in *Reath et al.* [2019a] and *Reath et al.* [2019b].

Figure S3

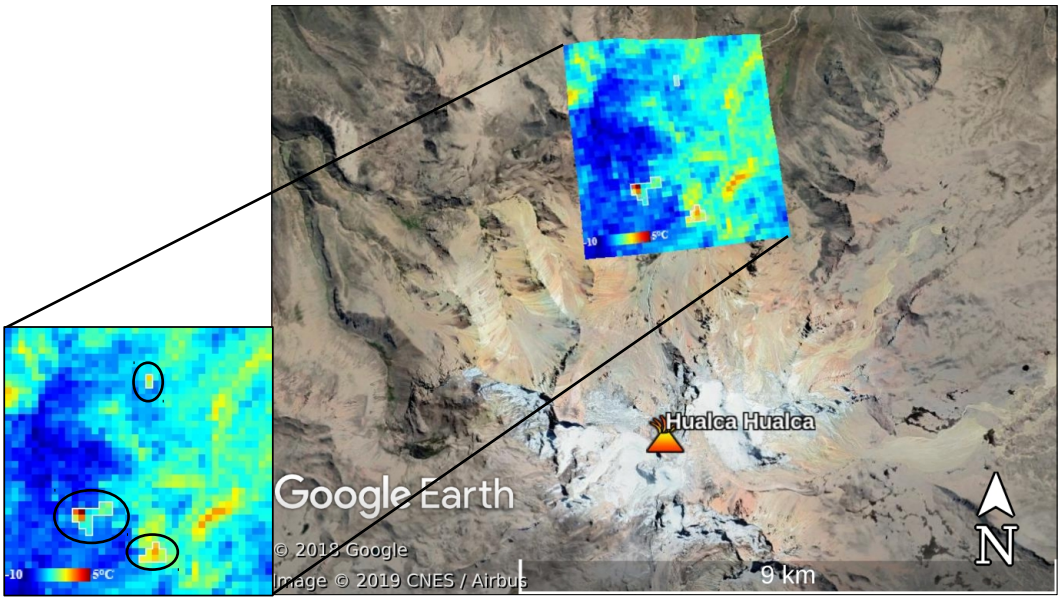

Figure S3. ASTER image from of thermal anomalies at Hualca Hualca acquired on May 17, 2018 at 03:25:22 UTC. Three thermal anomalies are marked by black ellipses, with pixels above background outlined in white. Regions with high temperatures that are not indicated as anomalies associated with topography or surface composition, see *Reath et al.* [2019b] for more detail on anomaly detection.

Figure S4

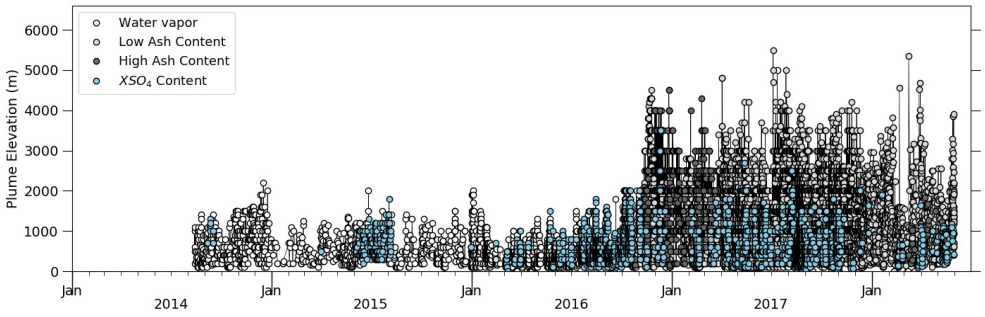

Figure S4. Observations of Sabancaya plume height and emission type from 2014 to 2018 derived from INGEMMET webcam monitoring. Plume heights are calculated based on known reference locations in the webcam images, and emission types are classified by the color of the plume. Data originally published in *Machacca Puma et al.* [2018].

Figure S5

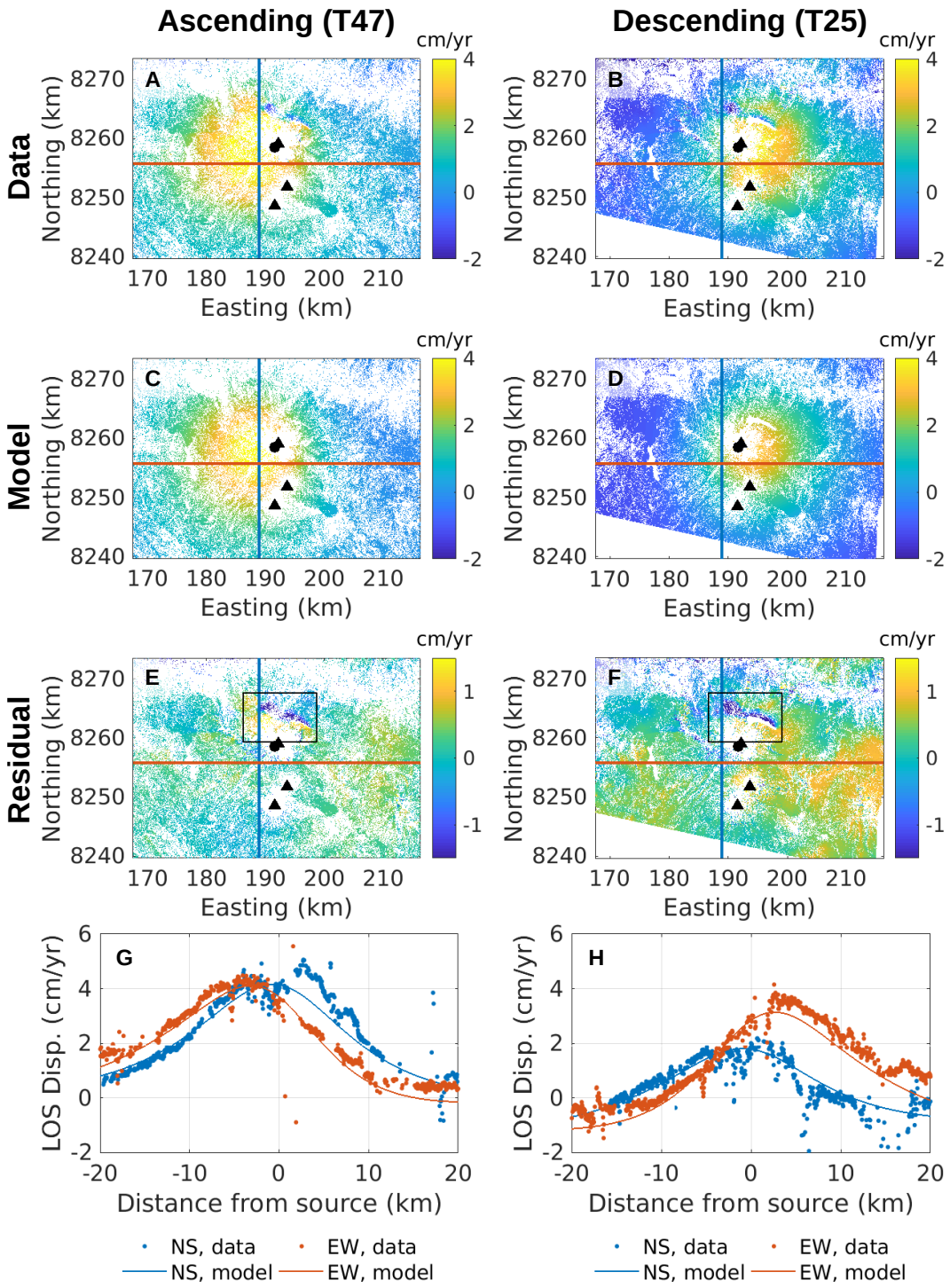

Figure S5. Prolate ellipsoidal source [*Yang et al.*, 1988, with corrections from *Newman et al.* [2006]] modeling results for inflation source, using rate maps from ascending and descending tracks for S-1 spanning 2014-2019. Top row is original data (full resolution), second row is forward modeled data, third row is the residual between the data and modeled data. The final row shows NS (orange) and EW profiles (blue) of data (dots) and forward modeled data (lines). Profiles are plotted as black lines in the first three rows. The deformation signals from the 2017 earthquakes (black rectangles in e and f) were not removed prior to inversion, as tests showed that removing them had no significant effect on the results for modeling the spherical source.

Figure S6

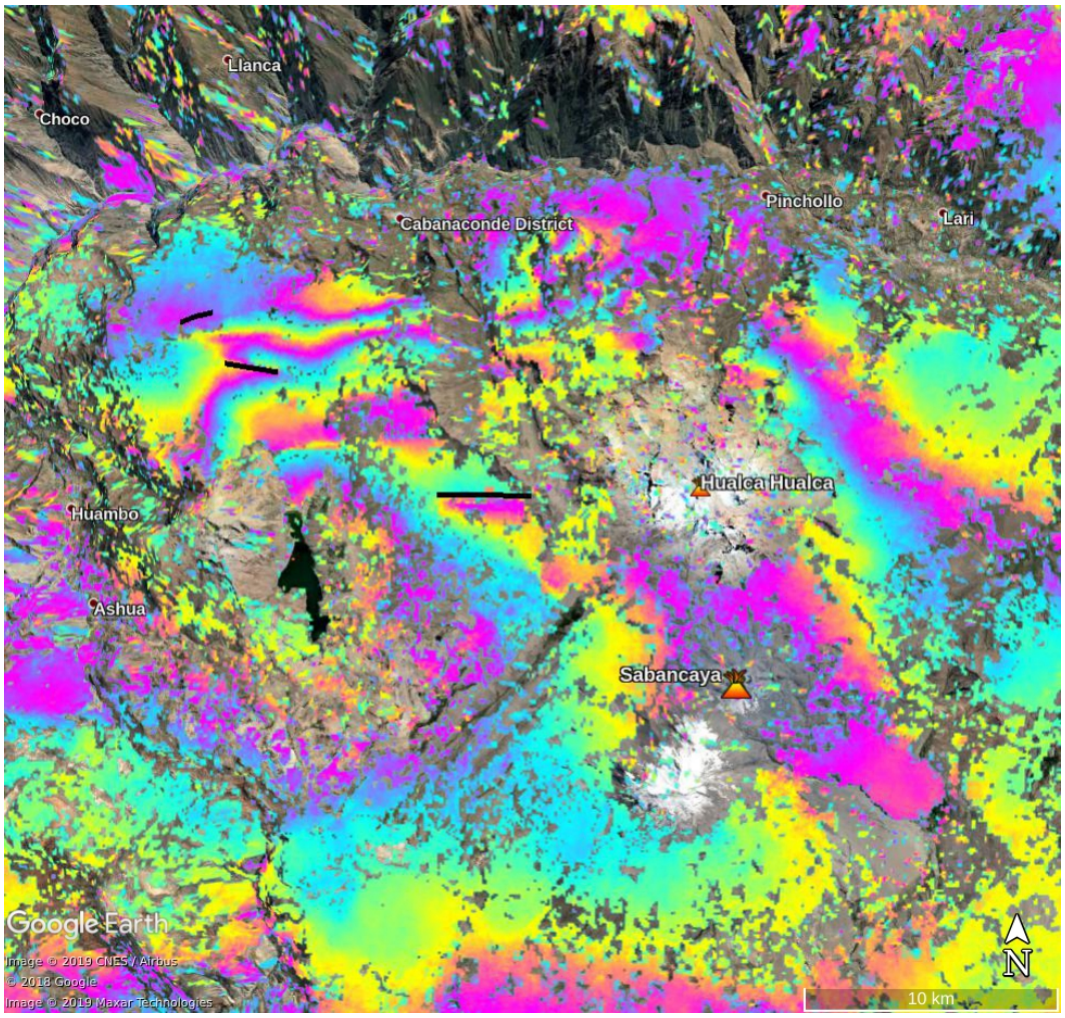

Figure S6. Google Earth overlay of ERS interferogram spanning 18 October 1996 to 27 September 2002 (Orbits 38885-07823), showing the 1998 Cabanaconde Earthquake (see also Fig. S7 of *Jay et al.* [2015]). Faults with triggered slip are marked with black lines.

Figure S7

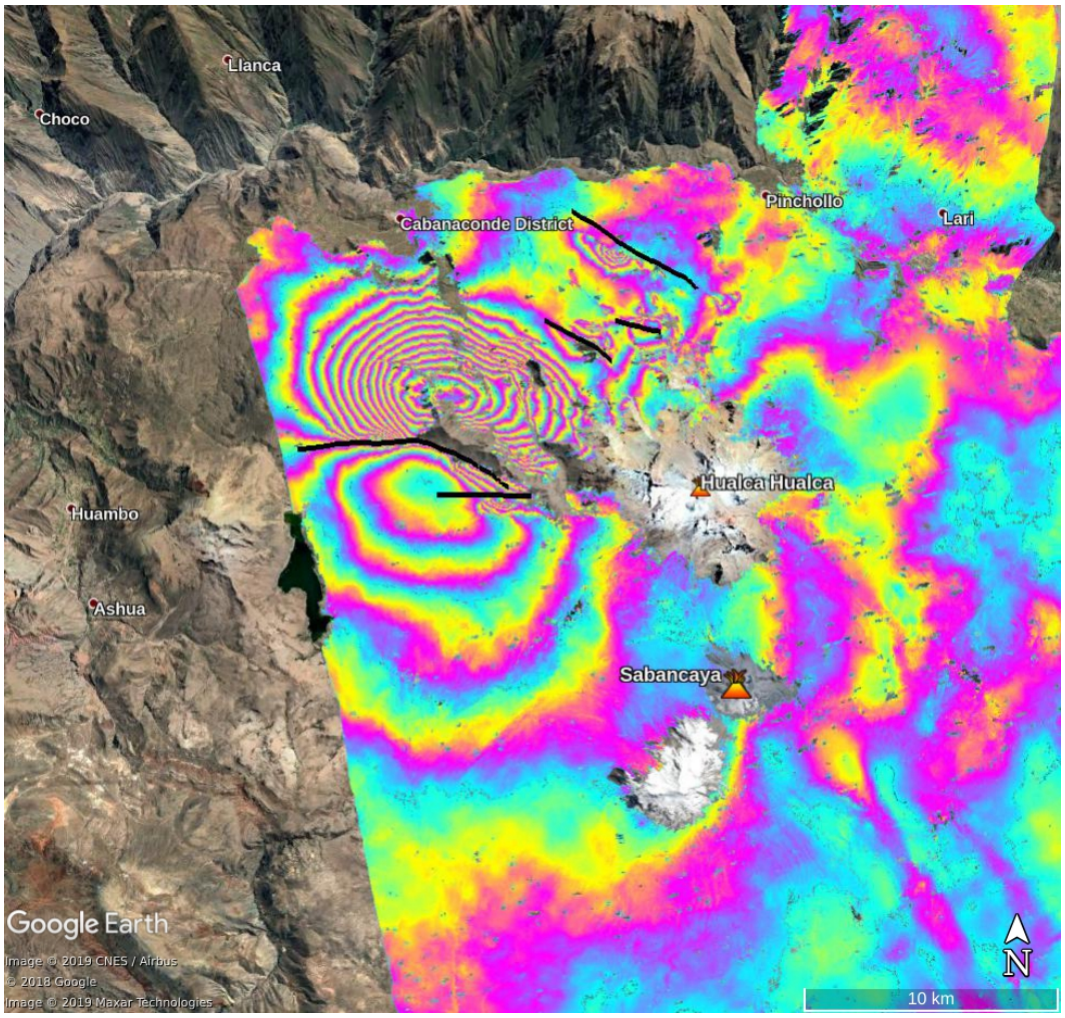

Figure S7. Google Earth overlay of TSX interferogram spanning 12 May 2012 to 17 July 2013 (Orbits 17047-16045), showing the 17 July 2013 M_W 5.9 earthquake. The M_W 5.9 fault and the other faults with triggered slip are marked with black lines.

Figure S8

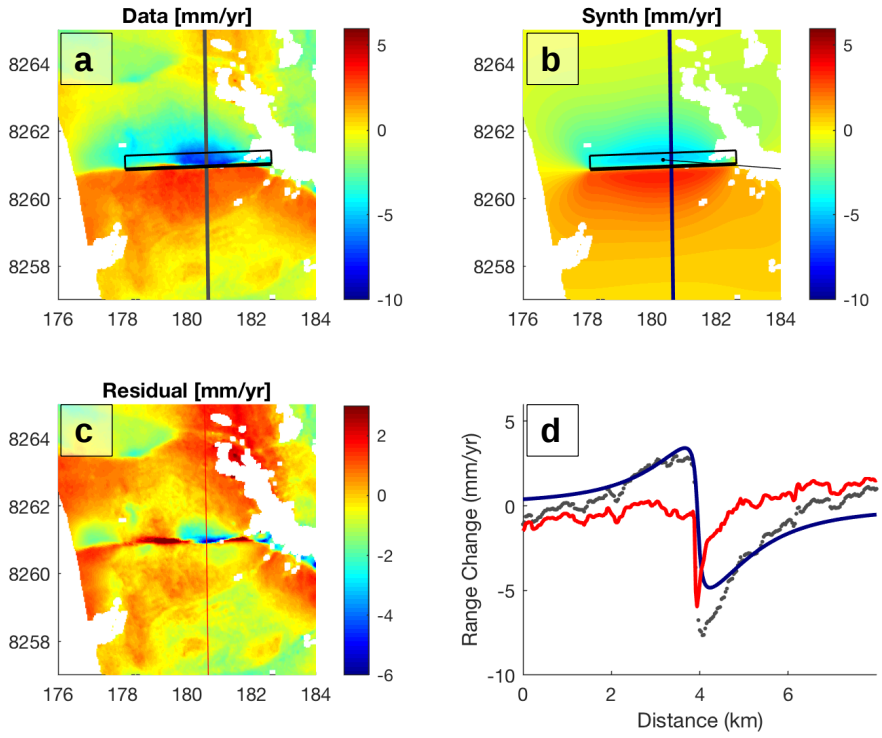

Figure S8. Modeling results for Creeping Fault 1 (Mojopampa Fault), using a surface deformation rate map calculated from the TSX time series (ascending) spanning November 2013 to December 2016. a) Full resolution data used for inversion. b) Predicted deformation from best-fit model geometry and slip. Modeled fault indicated with black box. c) Residual between data and predicted deformation. d) Profiles of range change for north-south profiles across the fault. Gray dots are original data (gray line in a), blue line is predicted data (blue line in b), and red line is the residual red line in c). Modeled fault plane indicated with black box in a) and b).

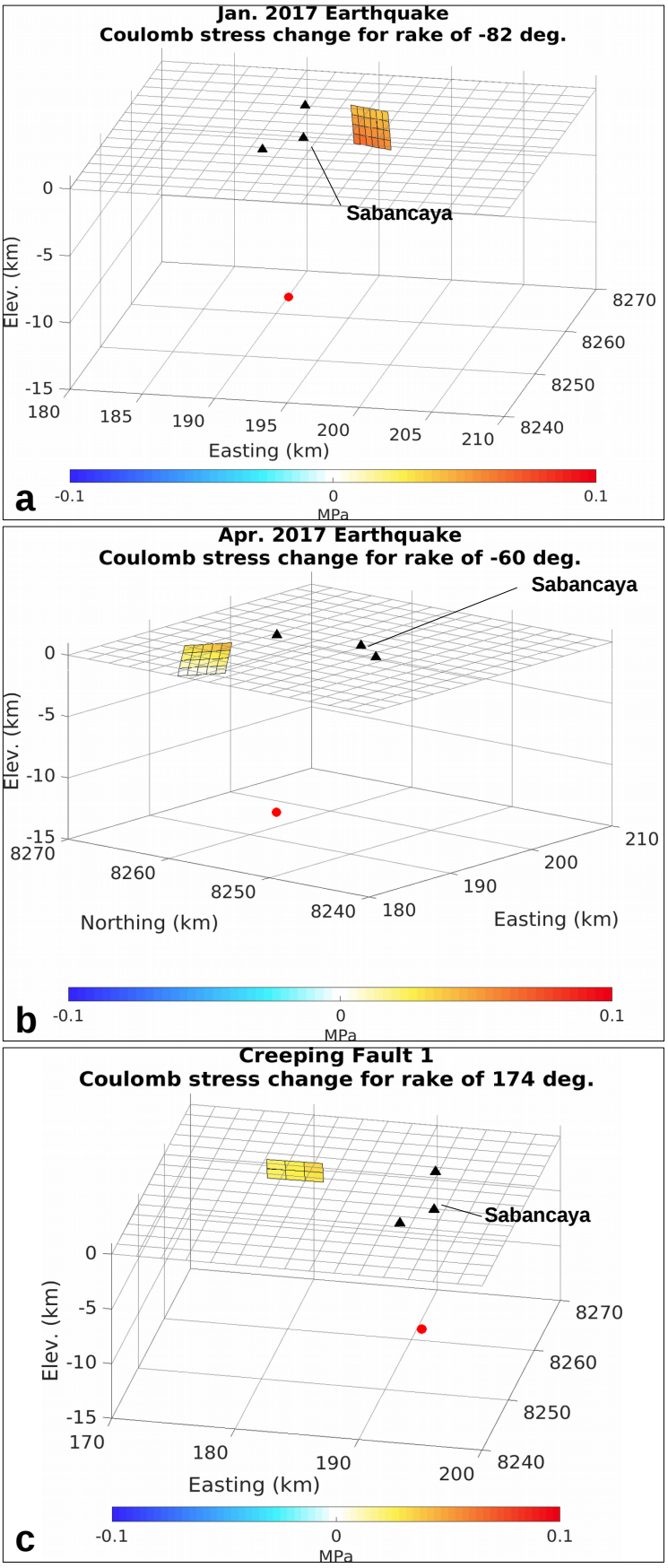

Figure S9. Coulomb static stress change for the 10 Jan. 2017 fault plane (a), 30 Apr. 2017 fault plane (b), and Creeping Fault 1 (c). Black triangles mark locations of volcanoes, and red circle marks the location of the modeled spherical inflation source.

Figure S10

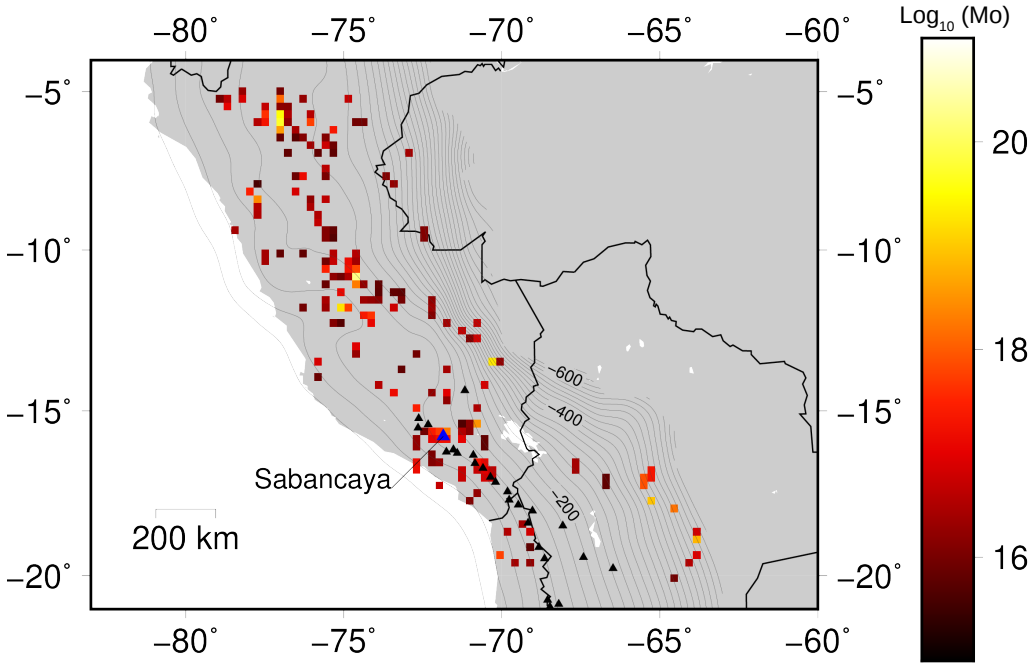

Figure S10. Map of log of cumulative seismic moment released from crustal earthquakes (depth < 30 km) 1800 to 2019. Earthquakes are taken from the NEIC Earthquake catalog, excluding earthquakes of M_W < 4.5 to minimize bias from uneven seismic station coverage in older epochs. Location of Sabancaya marked with large blue triangle, Holocene volcanoes with smaller black triangles [*Global Volcanism Program*, 2013]. Slab contours from *Hayes et al.* [2012].

Table S1

Satellite	Tracks	Num. Images	Dates Covered
ERS-1/2[1]	454 (Desc.)	17	2 June 1992 to 5 April 2002
Envisat[2]	454 (Desc.)	13	6 December 2002 to 19 March 2010
COSMO-SkyMed	N/A[3](Asc.)	96	9 March 2013 to 30 July 2014
TerraSAR-X[4]	43 (Asc., stripmap mode)	30	12 May 2013 to 22 December 2016
Sentinel 1 A/B	25 (Desc.), 47 (Asc.)	70, 77	19 October 2014 to 4 February 2019

[1] Data originally published in *Pritchard and Simons* [2004]

[2] Data originally published in *Jay* [2014] and *Jay et al.* [2015]

[3] CSK does not provide track/frame information.

[4] Data originally published in *Reath et al.* [2019a]

Table S1. Information on SAR satellite data used in this study

Table S2

	Interferogram Dates	
Earthquake	***Ascending (T47)***	***Descending (T25)***
January 10, 2017	16 Dec. 2016 to 19 Jan. 2017	6 Jan. 2017 to 30 Jan. 2017
April 30, 2017	8 Mar. 2017 to 19 May 2017	N/A

Table S2. Dates of interferograms used in 2017 earthquake modeling.

References

Global Volcanism Program (2013), Volcanoes of the World, v. 4.8.0., smithsonian Institution.

Hayes, G. P., D. J. Wald, and R. L. Johnson (2012), Slab1.0: A three-dimensional model of global subduction zone geometries, *Journal of Geophysical Research: Solid Earth*, *117*(B1), doi:10.1029/2011JB008524.

Jay, J. A. (2014), A Geophysical Survey of Active Volcanism in the Central and Southern Andes, Ph.D., Cornell University.

Jay, J. A., F. J. Delgado, J. L. Torres, M. E. Pritchard, O. Macedo, and V. Aguilar (2015), Deformation and seismicity near Sabancaya volcano, southern Peru, from 2002 to 2015,

Geophysical Research Letters, *42*(8), 2780–2788, doi:10.1002/2015GL063589.

Machacca Puma, R., M. A. Ortega Gonzáles, R. Miranda Cruz, F. E. Apaza Choquehuayta, I. A. Lazarte Zerpa, P. J. Masías Alvarez, D. A. Ramos Palomino, B. Ccallata Pacsi, R. M. Anccasi Figueroa, E. L. Taipe Maquerhua, and L. Cruz (2018), Monitoreo Multi-paramétrico del volcán Sabancaya y evolución del proceso eruptivo 2016-2017, in *Libro de resúmenes: VIII Foro Internacional los Volcanes y su Impacto, Arequipa, 26 y 27 de abril del 2018*, pp. 105–108, Instituto Geológico, Minero y Metalúrgico – INGEMMET, Arequipa, Peru.

Newman, A. V., T. H. Dixon, and N. Gourmelen (2006), A four-dimensional viscoelastic deformation model for Long Valley Caldera, California, between 1995 and 2000, *Journal of Volcanology and Geothermal Research*, *150*(1), 244–269, doi:10.1016/j.jvolgeores.2005.07.017.

Pritchard, M. E., and M. Simons (2004), An InSAR-based survey of volcanic deformation in the central Andes, *Geochemistry, Geophysics, Geosystems*, *5*(2), Q02,002, doi:10.1029/2003GC000610.

Reath, K., M. Pritchard, M. Poland, F. Delgado, S. Carn, D. Coppola, B. Andrews, S. K. Ebmeier, E. Rumpf, S. Henderson, S. Baker, P. Lundgren, R. Wright, J. Biggs, T. Lopez, C. Wauthier, S. Moruzzi, A. Alcott, R. Wessels, J. Griswold, S. Ogburn, S. Loughlin, F. Meyer, G. Vaughan, and M. Bagnardi (2019a), Thermal, Deformation, and Degassing Remote Sensing Time Series (CE 2000–2017) at the 47 most Active Volcanoes in Latin America: Implications for Volcanic Systems, *Journal of Geophysical Research: Solid Earth*, *0*(0), doi:10.1029/2018JB016199.

Reath, K., M. E. Pritchard, S. Moruzzi, A. Alcott, D. Coppola, and D. Pieri (2019b), The AVTOD (ASTER Volcanic Thermal Output Database) Latin America archive, *Journal of Volcanology and Geothermal Research*, *376*, 62–74, doi:10.1016/j.jvolgeores.2019.03.019.

Yang, X.-M., P. M. Davis, and J. H. Dieterich (1988), Deformation from inflation of a dipping finite prolate spheroid in an elastic half-space as a model for volcanic stressing, *Journal of Geophysical Research: Solid Earth*, *93*(B5), 4249–4257, doi:10.1029/JB093iB05p04249.